Structural and Multidisciplinary Optimization manuscript No.
(will be inserted by the editor)

Optimization of Dynamic Response using a Monolithic-Time Formulation

Mohammad H. Kurdi · Philip S. Beran

Received: date / Accepted: date

Abstract The design of systems for dynamic response may involve constraints that need to be satisfied over an entire time interval or objective functions evaluated over the interval. Efficiently performing the constrained optimization is challenging, since the typical response is implicitly linked to the design variables through a numerical integration of the governing differential equations. Evaluating constraints is costly, as is the determination of sensitivities to variations in the design variables.

In this paper, we investigate the application of a temporal spectral element method to the optimization of transient and time-periodic responses of fundamental engineering systems. Through the spectral discretization, the response is computed globally, thereby enabling a more explicit connection between the response and design variables and facilitating the efficient computation of response sensitivities. Furthermore, the response is captured in a higher order manner to increase analysis accuracy.

Two applications of the coupling of dynamic response optimization with the temporal spectral element method are demonstrated. The first application, a one-degree-of-freedom, linear, impact absorber, is selected from the auto industry, and tests the ability of the method to treat transient constraints over a large-time interval. The second application, a related mass-spring-damper system, shows how the method can be used to obtain work and amplitude optimal time-periodic control force subject to constraints over a periodic time interval.

Keywords Dynamic response optimization · spectral element · transient · periodic · path optimization · adjoint sensitivity · shape optimization

This research was performed while the first author held a National Research Council Research Associateship Award at the Air Force Research Laboratory.

An early version of this paper was presented at the 46th AIAA Aerospace Sciences Meeting and Exhibit, Jan 7–10, 2008, Reno, Nevada.

Air Force Research Laboratory, Air Vehicles Directorate, Building 146, 2210 Eighth Street, Wright-Patterson Air Force Base, Ohio 45433, USA.
Tel.: +937-25-57386, Fax: +937-65-64945,
E-mail: Mohammad.Kurdi@wpafb.af.mil; mhkurdi@gmail.com,
E-mail: Philip.Beran@wpafb.af.mil,

1 Introduction

Many engineering structures are subject to transient loading conditions. These structures must handle load variations for an entire time interval. To enforce the time-dependent constraints, the response needs to be evaluated accurately for an entire interval without missing any of the response extrema. Additionally, this evaluation needs to be efficient when an optimum design of the structure is sought because the objective, constraints and their sensitivities will need to be recomputed for each configuration visited by the optimizer.

The overwhelming majority of numerical techniques used to compute time-dependent responses are based on finite-difference schemes. In these methods, the solution of the governing second order differential equation is time-marched from the initial condition using small time steps until the dynamics reach a converged state. Here the time step size is crucial to the stability and accuracy of the computation and may limit its efficiency. Furthermore, the computational efficiency of these methods is more apparent when only the periodic response is of interest, where we need to integrate through many transient cycles to arrive at the steady-state cyclic response. This is particularly the case for systems with low damping. For these systems, frequency response analysis provides better alternative to computing the response [1, page 75] especially for harmonic actuation. However, for sharp excitations frequency-based methods are less accurate in resolving rapid variations in the response.

The use of time-marching methods in an optimization scheme is even more computationally intensive, where the time-dependent response is evaluated in small time-steps to eliminate constraint violation between any two time points. Additionally, in a gradient-based optimization search, the sensitivity of the response to design variables is required. The sensitivity can be computed using direct differentiation or adjoint method by defining a Lagrange multiplier [2, 3]. This computation is convoluted because the response is not explicit in the design variables. In both methods, the response sensitivity computation is hindered by another integration of the governing differential equations.

In the review by Kang et al. [4], the authors noted the advantage of using a finite element discretization of the time parameter. The attractive feature of the time finite element method [5, 6] is that it transforms the governing differential equation into an algebraic equation. This has the advantage of obtaining a more explicit connection of the response to the design variables, which in turn enables more efficient computation of the response sensitivity. In this paper, we use temporal spectral element method to discretize the time-dependent differential equation. The spectral element method, first introduced by Patera [7], combines the local flexibility of the finite element method with the accuracy of spectral methods. Within each element, a high order Lagrange polynomial is interpolated at time grid points corresponding to zeros of Gauss-Lobatto-Legendre (GLL) polynomials. The solution of the differential equation is computed for a monolithic-time interval which includes transient and steady-state response [8]. Similar discretization of the whole time interval using Hamilton's principle is found in [9, 10]. This is in contrast to a time-marching finite element approach [11, 12], where the response is computed in small time steps to steady-state. The discretization of the monolithic-time interval using the spectral elements provides local flexibility in resolving sharp transients in the response by increasing the polynomial order (p refinement) or decreasing element size (h refinement) near the sharp variation [8].

Early studies on the optimization of structures subject to transient loads goes back to the 1970s [13, 14]. This branch of optimization is referred to in the literature as dynamic response optimization [4]. Here, the time-dependent responses need to be evaluated for each iteration of the design variables and the constraints enforced for an entire time interval. There are several methods to apply time-dependent constraints. In an early work, Venkayya [15] applied the constraint only at the global minimum of the response. A more robust approach enforces the constraints at closely spaced points such that violation at intermediate points is unlikely [16]. This methodology is applied in a quasi-static manner in [17], where multiple equivalent static loads are enforced instead of the dynamic ones. In these approaches the number of constraints increase substantially. The optimization cost also increases because of the need to compute sensitivities of these constraints during the optimizer iterations. A more efficient procedure is to enforce the constraints only at the local extrema of the response critical to the design. This reduces the number of constraints and the resulting reduction in number of sensitivities calculations of the constraints with respect to the design variables [3, 18, 19].

The computation of the gradient in design optimization is essential in carrying out the search for an optimal design in an efficient manner [20]. The sensitivities can be computed using finite-difference, direct or adjoint methods [2, 21]. Efficiency of the last two methods depend on the number of constraints and design variables in the problem. The direct method is computationally more efficient when the number of constraints are larger than the number of design variables, whereas the adjoint method is more efficient when the converse is true. Problems where large number of design variables exist are in shape optimization [22–24], where the shape is parameterized using many design variables. It is in these applications, where the adjoint method is particularly attractive. In the second application of this paper we use this method to enable an efficient optimization search.

In this paper, we efficiently optimize the actuation of a dynamic system by computing monolithic-time responses and constraints with the temporal spectral element method. The discretization transforms the time dependence of the response into an explicit algebraic form, thereby allowing a more direct computation of the performance sensitivity. The sensitivities are computed using finite-difference, direct, and adjoint methods. We compare the optimization cost of enforcing the constraints at GLL points, where the solution is explicitly available, to the cost of enforcing the constraints at local extrema of the responses, which are identified using a one-dimensional, line-search method.

In this initial work, the new methodology is demonstrated by application to small-scale systems (low numbers of degrees-of-freedom). The extension to large-scale systems is important and will be addressed in future work. We note that dynamic responses have been efficiently computed with the temporal spectral element method for applications involving more than 60,000 variables [8]; problems of much larger size will require modifications to the basic analysis procedure to enable it to scale better with the numbers of degrees-of-freedom. However, these modifications ought not change the basic manner in which response sensitivities are computed or used in design optimization.

Two applications are described herein. The first application, derived from the auto industry, demonstrates method efficiency and accuracy for the transient response of linear systems. The second application, motivated by design of micro air vehicles, demonstrates the method for systems with periodic steady-state response and large numbers of design variables. The design variables are used to parameterize the actua-

tion force, where the optimization search is carried out by computing the gradients of the performance functions with the adjoint method.

2 Formulation of Dynamic Response Optimization Problem

The dynamic response optimization problem is to find the design variable vector $\boldsymbol{b}$ which

$$\begin{aligned} &\text{minimize} \quad c(\boldsymbol{b}, \boldsymbol{z}(t), \dot{\boldsymbol{z}}(t), \ddot{\boldsymbol{z}}(t), t), \\ \text{subject to} \quad & \\ &g_i(\boldsymbol{b}, \boldsymbol{z}(t), \dot{\boldsymbol{z}}(t), \ddot{\boldsymbol{z}}(t), t) \leq 0, \quad i = 1, ..., n \quad \forall t \in [0, T], \end{aligned} \tag{1}$$

where g_i is constraint number i and t is the time parameter and $\boldsymbol{z}$ is displacement vector which is the solution to

$$\begin{aligned} &\mathbf{M}\ddot{\boldsymbol{z}} + \mathbf{C}\dot{\boldsymbol{z}} + \mathbf{K}\boldsymbol{z} = \boldsymbol{f}, \\ &\boldsymbol{z}(0) = \boldsymbol{z}_0 \qquad \dot{\boldsymbol{z}}(0) = \dot{\boldsymbol{z}}_0, \end{aligned} \tag{2}$$

where $\mathbf{M}$, $\mathbf{C}$, $\mathbf{K}$ are the mass, damping and stiffness matrices. Note that the function g is an aggregate of the time-dependent response and the set-point of design constraint, consequently we refer to g as being time-dependent due to the time dependency of the response and not the design constraint point. Typically the solution of (2) is computed using time stepping schemes, where the spectral element expansion is applied on a small time step. In our approach we compute the response using a monolithic-time approach, where the entire time interval is discretized using the spectral element method. This transforms the time-dependent differential equation to an algebraic form and eliminates direct dependence on time. In the following we describe the temporal spectral element method which is used to apply the transformation.

3 Temporal Spectral Element Method

To apply the spectral element method (SE) [8] to the dynamic system described by (2); the set of second-order differential equations is transformed to first-order by introducing artificial variables. The coupled set of differential equations is,

$$\frac{\mathrm{d}x}{\mathrm{d}t} + \mathbf{A_s}x = f(x, t), \tag{3}$$

where x represents the collocated dependent variables $x \in R^{N_v}$, N_v is the number of dependent variables, time t is the independent variable, and $f(x, t)$ is a nonlinear function of x which can be time-dependent. The equations are coupled through the matrix $\mathbf{A_s}$, which is assumed to be time invariant.

In the following, the SE discretization of transient and time-periodic responses of (3) is described. The description is provided to review development of the SE method and emphasize the monolithic-time aspect in handling the dynamic constraints. This would enable application of the monolithic-time formulation in a gradient-based optimization of the dynamic response.

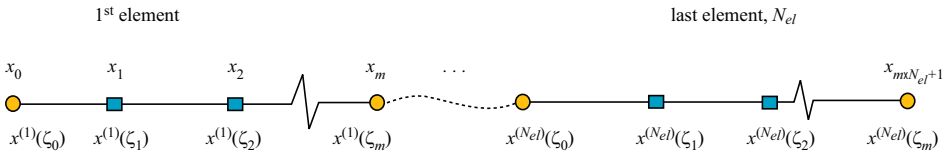

Fig. 1 Discretization of the time domain into N_{el} elements represented by an m order Lagrange polynomial within each element. Nodes of each element are placed at zeros of Lobatto polynomials.

3.1 Transient Analysis

Each dependent variable can be discretized in time using spectral elements [25], where the m^{th} order trial solution in each element is:

$$\hat{x}^{(j)}(\zeta) = \sum_{k=0}^{m} x^{(j)}(\zeta_k)\psi_k^{(j)}(\zeta). \tag{4}$$

Here $\psi_k^{(j)}$ represents the Lagrange polynomial of order k in element j, ζ_k are the zeros of the completed Lobatto-Legendre polynomials [26, page 143] defined on the interval $\zeta \in [-1, 1]$ with the first and last nodes corresponding to the element end points, and $x^{(j)}(\zeta_k)$ are the unknown nodal values placed at ζ_k for element j. The nodes locations allow for an expansion free of oscillations (in contrast to equi-spaced nodes) and efficient numerical implementation of Gauss-Legenre-Lobatto integration rule [25, page 50]. The physical time domain $t \in [t_j, t_{j+1}]$, see Fig. (1), is transformed to the ζ domain for each element. The Lobatto polynomials L_{o_i} are a set of orthogonal polynomials that can be defined as the derivatives of degree $i+1$ Legendre polynomials [26], L_{i+1}:

$$L_{o_i}(\zeta) \equiv L_{i+1}^{'}(\zeta), \tag{5}$$

where the Legendre polynomials are defined explicitly as

$$L_i(\zeta) = \frac{1}{2^i i!}\frac{\mathrm{d}^i(\zeta^2-1)^i}{\mathrm{d}\zeta^i}. \tag{6}$$

We review the development of SE here for completeness. Substituting the trial solution $\hat{x}^{(j)}$ into the differential equation (3) and minimizing the residual in each element using the Bubnov-Galerkin method [27] we have (assume A_s is scalar for now):

$$\sum_{j=1}^{N_{el}} \int_{-1}^{1} v(\zeta)\Big[\frac{\mathrm{d}\hat{x}^{(j)}}{\mathrm{d}\zeta} + \frac{h^{(j)}}{2}\Big\{A_s\hat{x}^{(j)} - f^{(j)}(\hat{x}^{(j)}, \zeta)\Big\}\Big]\,\mathrm{d}\zeta = 0, \tag{7}$$

where $h^{(j)}$ is the width of element j and $v(\zeta)$ is a weighting function taken as the p^{th} Lagrange polynomial, $\psi_p^{(j)}$. Integrating by parts we find for $p = 0, \ldots, m$:

$$\sum_{j=1}^{N_{el}} \left[\hat{x}^{(j)} \psi_p^{(j)} \Big|_{-1}^{1} - \int_{-1}^{1} \left(\hat{x}^{(j)} \frac{\mathrm{d}\psi_p^{(j)}}{\mathrm{d}\zeta} - \frac{h^{(j)}}{2} \left\{ A_s \hat{x}^{(j)} \psi_p^{(j)} - f^{(j)}(\hat{x}^{(j)}, \zeta) \psi_p^{(j)} \right\} \right) \mathrm{d}\zeta \right] = 0. \tag{8}$$

Exploiting the property of Lagrange polynomials, (8) is efficiently integrated using Gauss-Lobatto-Legendre quadrature rule according to:

$$\int_{-1}^{1} I \mathrm{d}\zeta = \sum_{q=0}^{m} I(\zeta_q) \omega_q, \tag{9}$$

where I is a generic function of ζ and ω_q is the Gaussian quadrature weight at node q. This gives the following compact matrix formulation for each element:

$$\mathbf{\Psi} \begin{Bmatrix} x(\zeta_0) \\ \vdots \\ x(\zeta_m) \end{Bmatrix}^{(j)} = A_s \mathbf{I}_{\omega}^{(j)} \begin{Bmatrix} x(\zeta_0) \\ \vdots \\ x(\zeta_m) \end{Bmatrix}^{(j)} - \mathbf{I}_{\omega}^{(j)} f^{(j)}, \tag{10}$$

where

$$\mathbf{\Psi} = \begin{bmatrix} \frac{\mathrm{d}\psi_0}{\mathrm{d}\zeta}\big|_{\zeta_0} \omega_0 + 1 & \frac{\mathrm{d}\psi_0}{\mathrm{d}\zeta}\big|_{\zeta_1} \omega_1 & \dots & \frac{\mathrm{d}\psi_0}{\mathrm{d}\zeta}\big|_{\zeta_m} \omega_m \\ \frac{\mathrm{d}\psi_1}{\mathrm{d}\zeta}\big|_{\zeta_0} \omega_0 & \frac{\mathrm{d}\psi_1}{\mathrm{d}\zeta}\big|_{\zeta_1} \omega_1 & \dots & \vdots \\ \vdots & \dots & \dots & \frac{\mathrm{d}\psi_{m-1}}{\mathrm{d}\zeta}\big|_{\zeta_m} \omega_m \\ \frac{\mathrm{d}\psi_m}{\mathrm{d}\zeta}\big|_{\zeta_0} \omega_0 & \dots & \frac{\mathrm{d}\psi_m}{\mathrm{d}\zeta}\big|_{\zeta_{m-1}} \omega_{m-1} & \frac{\mathrm{d}\psi_m}{\mathrm{d}\zeta}\big|_{\zeta_m} \omega_m - 1 \end{bmatrix}, \tag{11}$$

and

$$I_{\omega_{ij}}^{(j)} = \frac{h^{(j)}}{2} \delta_{ij} \omega_i, \qquad \text{where} \quad \delta_{ij} = 0 \quad \text{if} \quad i \neq j, \qquad \delta_{ij} = 1 \quad \text{if} \quad i = j. \tag{12}$$

Note that $\omega_p = \int_{-1}^{1} \psi_p(\zeta) \mathrm{d}\zeta$. In (11), the first and last diagonal elements of differentiation matrix $\mathbf{\Psi}$ have an additional term (=1) due to the first term in (8). After enforcing the essential inter-element continuity

$$x^{(j)}(\zeta_m) = x^{(j+1)}(\zeta_0), \tag{13}$$

the assembly of a global matrix from (10) for N_{el} spectral elements yields a compact, Galerkin projection governing the approximate solution in time (one dependent variable):

$$\mathbf{L}_c X_c = A_s \mathbf{L}_{\omega} X_c - \mathbf{L}_{\omega} F(X_c), \tag{14}$$

where $\mathbf{L}_c$ and $\mathbf{L}_{\omega}$ are the global differentiation and weight matrices, F is the global weighted form of the excitation and

$$X_c = \left[x\big|_{t_0} \; x\big|_{t_1} \; \dots \; x\big|_{t_{m \times N_{el}+1}} \right]^T, \tag{15}$$

is the SE solution of the dependent variable x collocated at all nodal times (redundant shared elements nodes are removed using (13)). It should be noted that the initial

condition is applied by replacing the first row and column of $\mathbf{L}_c$ with zeros except for the first element, which is replaced with one. Also, the first element in $\mathbf{L}_\omega$ is replaced with zero and the first element in $-\mathbf{L}_\omega F$ is replaced with the value of x at $t = 0$. The SE solution X_c in (14) can then be computed using iterative methods. However, for a strictly time-dependent forcing function (not function of X_c) both direct and iterative methods can be used, see Section 3.3.

3.2 Periodic Cyclic Analysis

In some problems, the interest lies in the steady-state time solution, where the response is time-periodic with a period, $T = 2\pi/\omega$, equal to the period of the forcing function. This occurs in damped systems with periodic forcing functions and in self-excited nonlinear systems exhibiting limit cycle oscillations (LCOs).

In these problems we are interested in the steady-state periodic solution only, where the time cycle is discretized spectrally in the same way as in the transient solution, however, assembly of global matrices $\mathbf{L}_c$ and $\mathbf{L}_\omega$ is different. Here the initial conditions do not affect the long term periodic solution. Additionally, periodicity of the array of elements is enforced by requiring that the end node in the last element to be the initial node of the first element:

$$x^{(1)}(\zeta_0) = x^{(N_{el})}(\zeta_m). \tag{16}$$

Contributions to the end node in the last element are added to contributions from first element. Consequently the last row and column of $\mathbf{L}_c$ are added to their counterpart in the first row and column. Therefore, the solution vector, X_c, becomes

$$X_c = \left[x\big|_{t_0} \; x\big|_{t_1} \; \dots \; x\big|_{t_{m\times N_{el}}} \right]^T. \tag{17}$$

3.3 Global Assembly and Solution

A number of dependent variables, N_v, can be handled through spatial connectivity matrix $\mathbf{A}_s$ of size $N_v \times N_v$. Here, the tensor product gives the global form of (14):

$$(\mathbf{I} \otimes \mathbf{L}_c)X_{cg} = (\mathbf{A}_s \otimes \mathbf{L}_\omega)X_{cg} - (\mathbf{I} \otimes \mathbf{L}_\omega)F_{cg}(X_{cg}), \tag{18}$$

where $\mathbf{I}$ is the identity matrix of size $N_v \times N_v$ and X_{cg} is a collocation of all dependent variables at nodal times grouped by their corresponding independent variables, N_v. For transient solution X_{cg} takes the form:

$$X_{cg} = \left[\begin{Bmatrix} x_1\big|_{t_0} \\ x_1\big|_{t_1} \\ \vdots \\ x_1\big|_{t_{m\times N_{el}+1}} \end{Bmatrix}^T \dots \begin{Bmatrix} x_{N_v}\big|_{t_0} \\ x_{N_v}\big|_{t_1} \\ \vdots \\ x_{N_v}\big|_{t_{m\times N_{el}+1}} \end{Bmatrix}^T \right]^T. \tag{19}$$

A compact form of (18) becomes

$$\mathbf{J}X_{cg} = -\mathbf{L}_{\omega g}F_{cg}(X_{cg}), \tag{20}$$

where

$$\mathbf{J} = \mathbf{L}_{cg} - \mathbf{A}_{cg}. \tag{21}$$

The solution X_{cg} of (20) can be computed using Newton's method. By identifying a residual R we can write (20) as

$$R = \mathbf{J}X_{cg} + \mathbf{L}_{\omega g}F_{cg}(X_{cg}). \tag{22}$$

A first order Taylor series expansion of the nonlinear formula (22) gives

$$R^{\nu+1} = R^{\nu} + \mathbf{J}\Delta X_{cg} + \mathbf{L}_{\omega g}\left[F_{cg}^{\nu+1} - F_{cg}^{\nu}\right]. \tag{23}$$

The solution X_{cg} is computed by iterating the residual, $R^{\nu+1}$ in (23) to zero. To facilitate convergence we use a relaxation parameter λ according to

$$X_{cg}^{\nu+1} = X_{cg}^{\nu} + \lambda\Delta X_{cg}. \tag{24}$$

Note that when the forcing function is linear (independent of X_{cg}), the last term and updated residual in (23) are zero and for $\lambda = 1$, the solution X_{cg} can be evaluated from (24) in one iteration.

4 Treatment of Time-Dependent Constraints

The time-dependent constraints can be enforced in two ways. The first one enforces the constraints at the GLL grid points since the the spectral element solution, X_{cg} at these points is readily available. The constraint in (2) becomes

$$g_i(\boldsymbol{b}, \boldsymbol{z}(t_j), \dot{\boldsymbol{z}}(t_j), \ddot{\boldsymbol{z}}(t_j), t_j) \leq 0, \quad i = 1, ..., n, \quad j = 1, ..., n_g, \tag{25}$$

where n_g is the total number of grid points. In this approach, the grid points need to be closely spaced to reduce potential of constraint violation between adjacent grid points. However, this causes the number of points or constraints to be excessively large and leads to an expensive design process. The second one enforces the time constraints at its most critical time points (extrema) [18, 19]. The constraint in (2) becomes

$$g_i(\boldsymbol{b}, \boldsymbol{z}(t_j), \dot{\boldsymbol{z}}(t_j), \ddot{\boldsymbol{z}}(t_j), t_j) \leq 0, \quad i = 1, ..., n, \quad j = 1, ..., n_c, \tag{26}$$

where n_c is the number of local extrema or critical points. Once an accurate low degree of freedom spectral element solution is constructed, the local extrema of the Lagrange polynomial within each element is found using a one dimensional optimization method. Note that the location of the critical time points may drift as $\boldsymbol{b}$ is iterated. Therefore the extrema locations are recomputed during the design process.

5 Sensitivity Analysis

The temporal spectral element method reduces the differential equation of motion to an algebraic form resembling static equations $Ku = f$. Assuming we are applying the constraints at one GLL point according to (25), we can write the constraint as

$$h = g(X_{cg}, b) \leq 0, \tag{27}$$

where for simplicity of discussion we assume h depends on one design variable b. The sensitivity of h to a change in b is

$$\frac{\mathrm{d}h}{\mathrm{d}b} = \frac{\partial g}{\partial b} + \boldsymbol{y}^T \frac{\mathrm{d}X_{cg}}{\mathrm{d}b}, \tag{28}$$

where $\boldsymbol{y}$ is a vector with components

$$y_i = \frac{\partial g}{\partial X_{cg_i}}. \tag{29}$$

The first term in (28) is usually zero or simple to evaluate. The second part can be computed directly by differentiating (20) with respect to b and collecting multipliers to the response sensitivity $\frac{\mathrm{d}X_{cg}}{\mathrm{d}b}$

$$(\mathbf{J} + \mathbf{L}_{\omega g}\mathbf{Q})\frac{\mathrm{d}X_{cg}}{\mathrm{d}b} = -\mathbf{L}_{\omega g}\frac{\partial F_{cg}}{\partial b} - \frac{\mathrm{d}\mathbf{J}}{\mathrm{d}b}X_{cg}, \tag{30}$$

where the matrix $\mathbf{Q}$ is

$$Q_{ij} = \frac{\partial F_{cg_i}}{\partial X_{cg_j}}. \tag{31}$$

Note that for a linear forcing function $\mathbf{Q} = 0$. The sensitivity is computed by solving (30) for $\frac{\mathrm{d}X_{cg}}{\mathrm{d}b}$ and substituting into (28). Alternatively, the sensitivity can be computed using the adjoint method [2, p. 265] without the need to compute the sensitivity of the response. By premultiplying (30) with a Lagrange multiplier $\boldsymbol{\lambda}$, adding it to (28) and collecting multipliers to the response sensitivity $\frac{\mathrm{d}X_{cg}}{\mathrm{d}b}$ we have

$$\frac{\mathrm{d}h}{\mathrm{d}b} = \frac{\partial g}{\partial b} + \left[\boldsymbol{y}^T + \boldsymbol{\lambda}^T(\mathbf{J} + \mathbf{L}_{\omega g}\mathbf{Q})\right]\frac{\mathrm{d}X_{cg}}{\mathrm{d}b} + \boldsymbol{\lambda}^T\left(\mathbf{L}_{\omega g}\frac{\partial F_{cg}}{\partial b} + \frac{\mathrm{d}\mathbf{J}}{\mathrm{d}b}X_{cg}\right), \tag{32}$$

where to eliminate the need to compute $\frac{\mathrm{d}X_{cg}}{\mathrm{d}b}$, the adjoint vector $\boldsymbol{\lambda}$ becomes the solution to

$$\boldsymbol{y}^T = -\boldsymbol{\lambda}^T(\mathbf{J} + \mathbf{L}_{\omega g}\mathbf{Q}). \tag{33}$$

The sensitivity is then computed by dropping out the term containing $\frac{\mathrm{d}X_{cg}}{\mathrm{d}b}$ in (32)

$$\frac{\mathrm{d}h}{\mathrm{d}b} = \frac{\partial g}{\partial b} + \boldsymbol{\lambda}^T\left(\mathbf{L}_{\omega g}\frac{\partial F_{cg}}{\partial b} + \frac{\mathrm{d}\mathbf{J}}{\mathrm{d}b}X_{cg}\right). \tag{34}$$

The choice of the constraint(s) sensitivity computation method depends on the number of constraints and design variables [2, p. 267]. When the number of constraints is larger than the number of design variables it is more efficient to use the direct method by solving (30) for $\frac{\mathrm{d}X_{cg}}{\mathrm{d}b}$ once for each design variable and substituting into (28). Otherwise, when the number of design variables is larger, the adjoint method is more efficient to use by computing the adjoint vector in (33) once for each constraint and substituting into (34).

6 Results and Discussion

Two example problems are employed to demonstrate dynamic response optimization for transient and periodic analysis. The transient and periodic time intervals are discretized using the SE method to transform the set of differential equations to an algebraic form. The solution of the system of equations (20) gives an accurate representation of the global time response. This facilitate the application of time dependent constraints in design optimization, where the constraints may be applied anywhere in time. Additionally, the availability of the global response enables the computation of global sensitivity using direct or adjoint methods.

As mentioned in Section 4, the time dependent constraints may be applied only at the local extrema or at many locations in time. In the impact absorber problem we analyze constraint enforcement strategies on the accuracy of the optimal designs and the efficiency of the SE method. Finally, the global SE scheme is applied to the control force design of a dynamic system with many design variables to demonstrate application of adjoint sensitivity analysis.

6.1 Impact Absorber

We describe an example of the dynamic response for a single-degree-of-freedom linear impact absorber studied by Etman et al. [28]. The optimization problem is solved using the analytical solution and a spectral element approximation of the solution in time. The analytical solution is used to evaluate the accuracy of the temporal spectral element approach. In this example we compare two approaches for applying the time-dependent constraints with regard to accuracy and efficiency. In the first one, the constraints are enforced at the Gauss-Lobatto-Legendre, GLL, grid points. Here large number of points are needed to reduce greatly opportunity for constraint violation between any two adjacent points. In the second approach, we enforce the constraints only at the global minimum of the time response. This comparison is provided to show the computational cost incurred and design accuracy of both approaches.

The impact absorber is modeled as a single degree of freedom system with a mass M, linear stiffness K and linear damping coefficient C see Figure 2. The differential equation describing the motion of the absorber mass for zero initial displacement and velocity of 1 m/s is

$$M\ddot{z} + C\dot{z} + Kz = 0, \qquad z(0) = 0 \text{ m}, \qquad \dot{z}(0) = 1 \text{ m/s}. \tag{35}$$

The analytical solution of (35) for different combinations of stiffness and damping is

$$z(K,C,M,t) = \begin{cases} \frac{e^{-t\frac{C}{2M}}}{\sqrt{\frac{K}{M}-(\frac{C}{2M})^2}} sin\left(t\sqrt{\frac{K}{M}-(\frac{C}{2M})^2}\right), & \text{if } 0 \leq \frac{C/(2M)}{\sqrt{K/M}} < 1; \\ te^{-t\sqrt{\frac{K}{M}}}, & \text{if } \frac{C/(2M)}{\sqrt{K/M}} = 1; \\ \frac{e^{-t\frac{C}{2M}}}{2\sqrt{(\frac{C}{2M})^2-\frac{K}{M}}}\left[e^{t\sqrt{(\frac{C}{2M})^2-\frac{K}{M}}} - e^{-t\sqrt{(\frac{C}{2M})^2-\frac{K}{M}}}\right], & \text{if } \frac{C/(2M)}{\sqrt{K/M}} > 1; \end{cases} \tag{36}$$

For a fixed mass of the impact absorber ($M = 1$ kg), the optimization problem of the absorber is to find the stiffness b_1 and damping coefficient b_2 combination that

minimizes the maximum acceleration of the mass in the time interval $t \in [0, T]$

$$f(\boldsymbol{b}) = max|\ddot{z}(\boldsymbol{b}, t)|, \tag{37}$$

subject to the time displacement constraint

$$g(\boldsymbol{b}) = |z(\boldsymbol{b}, t)| - 1 \leq 0 \qquad \forall t \in [0, T], \tag{38}$$

and side constraints of the design variables

$$0 \leq \boldsymbol{b} \leq 1. \tag{39}$$

We note here that the time constraint has to be satisfied for a time interval. A time period $T = 12$ s is used which includes all important response characteristics. A graphical representation of the optimization problem is depicted in Figure 3. The maximum acceleration contours are plotted with the displacement constraint. The hatched part of the displacement constraint denotes the region where the constraint is violated. The design which minimizes the maximum acceleration is where the constraint intersects the minimum value of the objective function. For computational purposes the optimization problem is reformulated by minimizing an artificial design variable b_3 [29]

$$f(\boldsymbol{b}) = b_3, \tag{40}$$

subject to acceleration and displacement constraints

$$\begin{aligned} g_1(\boldsymbol{b}) &= \ddot{z}(b_1, b_2, t) - b_3 \leq 0, \\ g_2(\boldsymbol{b}) &= -\ddot{z}(b_1, b_2, t) - b_3 \leq 0, \\ g_3(\boldsymbol{b}) &= z(b_1, b_2, t) - 1 \leq 0, \\ g_4(\boldsymbol{b}) &= -z(b_1, b_2, t) - 1 \leq 0, \end{aligned} \tag{41}$$

where

$$0 \leq b_1 \leq 1, \quad 0 \leq b_2 \leq 1, \quad b_3 \geq 0, \quad \forall t \in [0, 12].$$

The optimum design is first computed using the analytical solution in (36). The time constraints in (41) are applied at the most critical point in the displacement and acceleration responses. The critical point is found by implementing a one dimensional optimization search. The optimization search method is the sequential quadratic programming (SQP) algorithm which is implemented using the *fmincon* function in Matlab® [30]. The accuracy in the objective, constraints and design variables is set to 1×10^{-15} in the main optimization and for locating the critical point. Note that the location of the critical time point is not constant and will continue to change as the design variables change. The optimum design, $\boldsymbol{b}_{\text{analytic}} = \{0.3606 \text{ N/m}, 0.4851 \text{ N.s/m}, 0.5206 \text{ m/s}^2\}$, is noted with green circle in Figure 3. This design is used to compare the accuracy of the design obtained when the temporal spectral element method is used to compute the acceleration and displacement responses.

The spectral element solution of (35) is computed by transforming the second order differential equation to first order. To facilitate this we introduce variables $z_1 = \dot{z}$ and $z_2 = z$ into (35) to get

$$\begin{Bmatrix} \dot{z_1} \\ \dot{z_2} \end{Bmatrix} + \begin{bmatrix} M & 0 \\ 0 & 1 \end{bmatrix}^{-1} \begin{bmatrix} C & K \\ -1 & 0 \end{bmatrix} \begin{Bmatrix} z_1 \\ z_2 \end{Bmatrix} = \begin{Bmatrix} 0 \\ 0 \end{Bmatrix}, \tag{42}$$

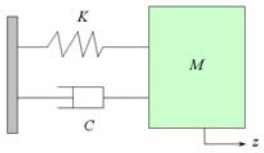

Fig. 2 Impact absorber.

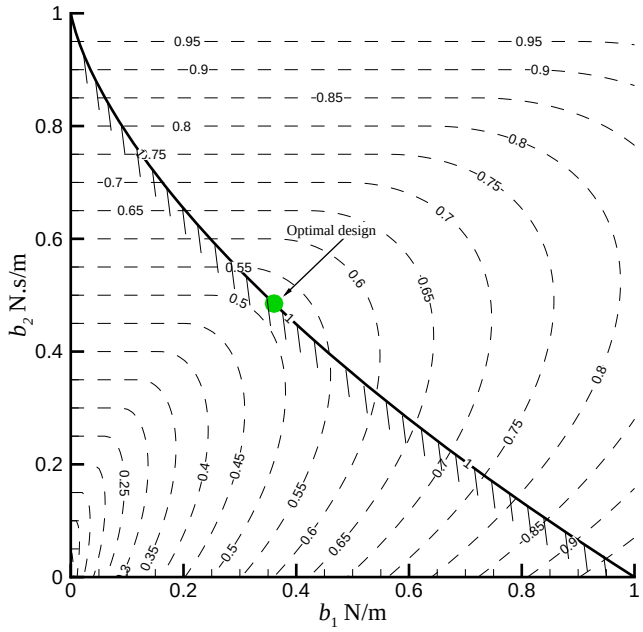

Fig. 3 Acceleration amplitude contours (dashed lines) and displacement amplitude constraint (solid line) for impact absorber. The optimum design is noted by green circle.

and after matrix multiplication, the first order form becomes

$$\begin{Bmatrix} \dot{z_1} \\ \dot{z_2} \end{Bmatrix} + \begin{bmatrix} C/M & K/M \\ -1 & 0 \end{bmatrix} \begin{Bmatrix} z_1 \\ z_2 \end{Bmatrix} = \begin{Bmatrix} 0 \\ 0 \end{Bmatrix}. \tag{43}$$

The acceleration response, $\dot{z}_1$, needed for the objective function evaluation can be computed from (43) after computing the velocity and displacement responses.

The constraints in (41) can then be written as

$$\begin{aligned} g_1(\boldsymbol{b}) &= \dot{z_1}(b_1, b_2, t) - b_3 \leq 0, \\ g_2(\boldsymbol{b}) &= -\dot{z_1}(b_1, b_2, t) - b_3 \leq 0, \\ g_3(\boldsymbol{b}) &= z_2(b_1, b_2, t) - 1 \leq 0, \\ g_4(\boldsymbol{b}) &= -z_2(b_1, b_2, t) - 1 \leq 0, \end{aligned} \tag{44}$$

where,

$$0 \leq b_1 \leq 1, \quad 0 \leq b_2 \leq 1, \quad b_3 \geq 0, \quad \forall t \in [0, 12].$$

From (42) and using the chain rule the sensitivities of g_1 and g_3 are

$$\begin{aligned} \frac{\partial g_1}{\partial b_1} &= -\frac{1}{M}(z_2 + b_1 \frac{\partial z_2}{\partial b_1} + b_2 \frac{\partial z_1}{\partial b_1}), & \frac{\partial g_3}{\partial b_1} &= \frac{\partial z_2}{\partial b_1}, \\ \frac{\partial g_1}{\partial b_2} &= -\frac{1}{M}(z_1 + b_2 \frac{\partial z_1}{\partial b_2} + b_1 \frac{\partial z_2}{\partial b_2}), & \frac{\partial g_3}{\partial b_2} &= \frac{\partial z_2}{\partial b_2}, \\ \frac{\partial g_1}{\partial b_3} &= \{-1\}, & \frac{\partial g_3}{\partial b_3} &= \{0\}. \end{aligned} \tag{45}$$

The sensitivity is computed by the adjoint method using (34) by solving for the adjoint vector once for the two constraints (g_1 and g_3).

In the initial spectral element implementation, the time constraints are monitored only at GLL points. In this procedure we may need to use large number of time grid points (large N_{el} and m) in order to capture the extremum of the response, although high accuracy of the SE solution can be achieved using 25 DOFs [8]. In Table 1, the infinity error norm of the optimum design $||\boldsymbol{b} - \boldsymbol{b}_{\text{analytic}}||_\infty$ is reported along with the corresponding computational time for different number of elements and Lagrange polynomial order. Note that the accuracy of the SE solution (not reported in the table) increases with increase in m or N_{el}. However, the accuracy of the design fluctuates and largely depends on whether a particular grid point is at the maximum of the response. For example, Figure 4a shows grid points for one element and degree eleven Lagrange polynomial, where none of the grid points were located at the maximum of the response. During design iterations the grid points may come close to the maximum response, though this situation cannot be predicted in advance of the design process, an example of this is reported in Figure 4b at the optimum design. The best accuracy was obtained at $N_{el} = 105$ and $m = 3$. The computational time of the optimization run for forward finite-difference and adjoint sensitivity computation is additionally noted. The latter method is slightly more efficient than the finite-difference perturbation of the responses. Though, for larger number of design variables, the cost savings of the adjoint approach is still realizable. This is because, the cost of the adjoint sensitivity is dominated by the computational cost of computing the adjoint vector using (33), which is independent of the number of design variables. The reported time corresponds to a computation using Matlab [30]*backslash* operator, which uses an LU factorization based on Gaussian elimination.

Alternatively, we can apply the time constraints only at the critical points of the time response while the response is computed using minimal number of degrees of freedom corresponding to an acceptable accuracy at each grid point. To find the critical times, we use a one dimensional optimization search to locate the local extrema of the corresponding Lagrange polynomial within each element, see the one element solution in Figure 4. Here the *fmincon* function is used with the accuracy in the objective

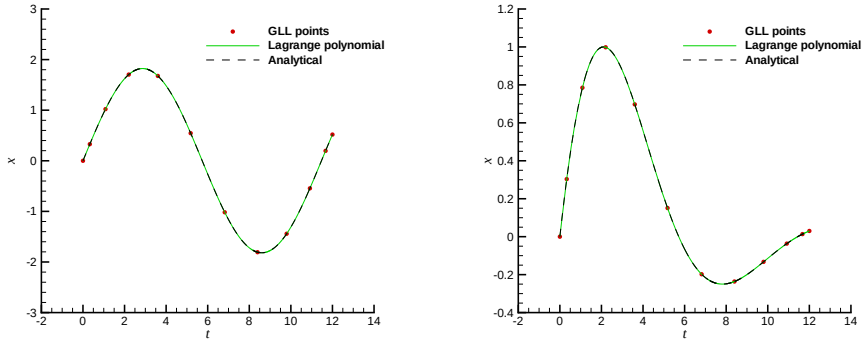

(a) Response for $b_1 = 0.3$ N/m and $b_2 = 0.001$ Ns/m.

(b) Response at optimum design $b_1 = 0.3606$ N/m and $b_2 = 0.4851$ Ns/m.

Fig. 4 Underdamped response of impact absorber. The uneven spacing of GLL grid points for an eleven degree polynomial element are noted.

Table 1 Infinity error norm of the design when the constraints and objective are evaluated at the GLL nodal points. The analytic design corresponds to the design computed using critical time points with analytical objective and constraints. The CPU computation time is noted.

		$\|\|\frac{\boldsymbol{b}-\boldsymbol{b}_{\text{analytic}}}{\boldsymbol{b}_{\text{analytic}}}\|\|_\infty$ %									
		N_{el}									
		5	30	55	80	105	130	155	180	205	230
m	1	177.320	2.146	2.357	2.701	1.449	0.391	0.399	0.951	1.032	0.432
	2	12.177	2.784	0.519	1.545	0.800	0.176	0.188	0.456	0.663	0.101
	3	10.453	0.434	1.015	0.377	0.065	0.462	0.323	0.081	0.195	0.463
Adjoint sensitivity - CPU time, s											
m	1	0.1	0.5	0.3	0.5	0.7	0.7	0.9	1.4	1.3	1.6
	2	0.1	0.3	0.6	1.1	1.3	2.2	2.5	3.2	4.0	5.1
	3	0.1	0.5	0.8	2.0	3.0	4.2	6.1	8.2	8.8	10.7
finite-difference sensitivity - CPU time, s											
m	1	0.1	0.5	0.4	0.7	0.9	1.0	1.2	1.7	1.7	2.1
	2	0.2	0.4	0.7	1.5	1.8	2.7	3.2	3.8	4.9	5.9
	3	0.2	0.6	1.1	2.6	3.4	4.8	7.5	9.4	10.6	12.9

and time design variable being set to 1×10^{-15} for the critical point search. The constraint is then enforced at each local minimum. To locate all the local extrema we run *fmincon* with multiple initial guesses corresponding to the grid points close to these extrema. However, for this problem, there is only one global minimum and we apply the constraint at this point only whilst the location of this point will be updated as the design variables change during optimizer iterations. Table 2, reports the infinity error norm of the computed design and the corresponding computational time for combinations of Lagrange polynomial order and number of elements. The data indicate that the accuracy and efficiency improved substantially with small number of elements and polynomial degree in comparison to the previous approach. Particularly, the design

Table 2 Infinity error norm of the design when the global minimum approach is used to enforce the constraints with finite difference sensitivity. The temporal spectral element method is used to compute the responses. The analytic design corresponds to the design computed with analytical objective and constraints. The CPU computation time is noted.

		$\|\|\frac{\boldsymbol{b}-\boldsymbol{b}_{\text{analytic}}}{\boldsymbol{b}_{\text{analytic}}}\|\|_\infty$ %					CPU time, s				
		m					m				
		6	8	10	12	14	6	8	10	12	14
N_{el}	1	1.8×10^{2}	3.0×10^{-1}	2.2×10^{-2}	8.6×10^{-4}	9.3×10^{-6}	2.1	2.3	2.4	2.9	2.7
	2	1.6×10^{-1}	3.2×10^{-3}	2.5×10^{-5}	1.0×10^{-6}	1.9×10^{-7}	2.4	2.6	2.5	2.9	3.0
	3	1.2×10^{-2}	8.6×10^{-5}	1.6×10^{-6}	2.0×10^{-6}	8.3×10^{-7}	2.5	2.5	2.9	3.0	3.2

was accurate to 1.9×10^{-9} with $m = 14$ and $N_{el} = 2$. This indicates superiority of applying time-dependent constraints at the critical extrema of the response with regard to computational cost and accuracy.

6.2 Control Force Design Considering Minimum Work

An interesting application of dynamic response optimization is in the design of micro air vehicles (MAV) [31–33]. One aspect in the design of MAV is the selection of a control force that minimizes utilization of actuation work [34, 35]. A simplified model of the MAV is a mass-spring-damper system. When the system is linear, the long time response of the underdamped system is independent of the initial conditions. The response to a periodic actuation force is governed by the differential equation

$$M\ddot{z} + C\dot{z} + Kz = f(t+T), \tag{46}$$

where T is the period of the actuation force f. Writing Eq. 46 in scaled time $s \in [0, 1]$

$$\frac{1}{T^2}M\ddot{z} + \frac{1}{T}C\dot{z} + Kz = f(s), \tag{47}$$

where $\dot{z}$ is now the derivative with respect to s. To compute the response z using the SE method, Equation 47 is written in first-order form similar to (42)

$$\frac{1}{T^2}\begin{Bmatrix}\dot{z_1}\\ \dot{z_2}\end{Bmatrix} + \begin{bmatrix}M & 0\\ 0 & 1\end{bmatrix}^{-1}\begin{bmatrix}\frac{C}{T} & K\\ -\frac{1}{T^2} & 0\end{bmatrix}\begin{Bmatrix}z_1\\ z_2\end{Bmatrix} = \begin{bmatrix}M & 0\\ 0 & 1\end{bmatrix}^{-1}\begin{Bmatrix}f(s)\\ 0\end{Bmatrix}. \tag{48}$$

The minimum work per cycle objective is motivated by the MAV, where an optimal actuation force is favorable to achieve a prescribed maximum displacement amplitude with the least amount of work. For the mass-spring-damper system, the optimization problem is to find the period, T and functional form of the control force that minimizes the exerted work for a specified set of target steady-state displacement amplitudes, Z_{T_i}

$$\min_{T,F_d} \quad W \qquad d = 1, ..., n_d - 1, \tag{49a}$$

subject to

$$\max(|z|) \geq Z_{T_i} \qquad i = 1, ..., N, \tag{49b}$$

$$|F_d| \leq 1, \tag{49c}$$

$$\frac{T_n}{4} < T \leq 1.5T_n, \tag{49d}$$

where the upper bound for the forcing period is restricted to less than an integer multiple of T_n to eliminate the possibility of repeated designs of the forcing period and W is the amount of external work per cycle exerted by $f(s)$

$$W = \int_0^1 f(s)\dot{z}ds, \tag{50}$$

and F_d is the magnitude of the control force at design node d, n_d is the total number of design variables which include the period T and T_n is the natural period of the system. The response in (48) is computed according to (20). The integrand in (50) can be written using a spectral representation

$$W = \int_0^1 \{F_g \cdot X_{cg}\}ds, \tag{51}$$

where "$\cdot$" denotes the dot product and the first $N_{el} \times m$ cells of F_g are the GLL nodal values of the control force, with the remaining $N_{el} \times m$ cells equal to zero, F_g is related to F_{cg} in (20) according to

$$F_{cg} = \begin{bmatrix} M & 0 \\ 0 & 1 \end{bmatrix}^{-1} \begin{Bmatrix} 1 \\ 0 \end{Bmatrix} \otimes F_g. \tag{52}$$

The actuation force $f(s)$ is modeled using a cubic spline discretization. This ensures first derivative continuity of the force and makes the accurate time integration less costly. The alternative option of discretizing the force at all the GLL points results in inaccurate time integration, where perturbations in the actuation force (design variables) during design iterations would result in sharp variations in the actuation force at interelement nodes. Sharp change in the actuation force may not be realizable and may cause inaccuracies in the time integration resulting in an erroneous optimization search. Note that an increase in the number of elements will only deteriorate time integration accuracy by allowing extra points of sharp change. The spline simulation of the actuation force is constructed by enforcing C^1 continuity at a number of nodes on the scaled time interval of [0,1]. Design points are assigned to the magnitude of the actuation force at each node. Since we are implementing a periodic analysis, the magnitude of the force at the left boundary node ($s = 0$) must be equal to the one at the right boundary node ($s = 1$). This can be enforced by assigning the same design variable to both nodes at $s = \{0, 1\}$.

The number of nodes is selected to enable an accurate construction of different variations of the actuation force. This allows for the precise interpolation of the force magnitude to the GLL grid points. For example, when 10 design points are used to construct the function $\arctan(10 \sin 2\pi s)/1.5$ (Figure 5a), there exist large differences

between the original function and the spline fitted one. This error will result in an error in the value of function at the GLL grid points (F_{cg}). When the number of design points is increased, the interpolation error is reduced, see Figure 5b, and the spectral element solution accuracy is improved.

The GLL values of control force, F_g are computed using a spline interpolation

$$F_g = \begin{Bmatrix} \{\boldsymbol{R}F_d\}_{N_{el}\times m} \\ \{0\}_{N_{el}\times m} \end{Bmatrix}, \tag{53}$$

where $\boldsymbol{R}$ is the spline transformation matrix. However, the number of GLL points must be adequate in reconstructing the actual actuation force represented by the spline. This is particulary important when design perturbations of design points lead to an actuation force with high frequency content, where we need to ensure the convergence of the SE discretization in all of the control force design space. Consider for example the spline representation of the harmonic $\sin 2\pi s$. The spline is constructed using 51 design points ($n_d = 51$, with one design variable reserved for the control force period) using the values $\sin 2\pi s_d$. A spectral discretization using a Lagrange polynomial of order $m = 5$ and $N_{el} = 5$ (25 grid points) is used to construct the $\sin 2\pi s$ signal. Figure 6a, illustrate good accuracy of the signal reconstruction using the 25 GLL grid points as seen by the overlapping of the spline and Lagrange interpolations. In the design optimization search the design variables are frequently perturbed. This can be simulated by adding a Gaussian noise of $N(\mu, \sigma)\delta$ with $\delta = 0.2$, $\mu = 0$ and $\sigma = 1$ to each design point. This results in a high frequency actuation force. Now, when the 25 GLL grid points are used to reconstruct the actuation force significant error is introduced, see Figure 6b. The error is due to insufficient number of GLL grid points for the iterated design. The error is reduced by ensuring that the number of GLL grid points are at least equal to the number of control force design points ($n_d - 1$), see Figrue 6c.

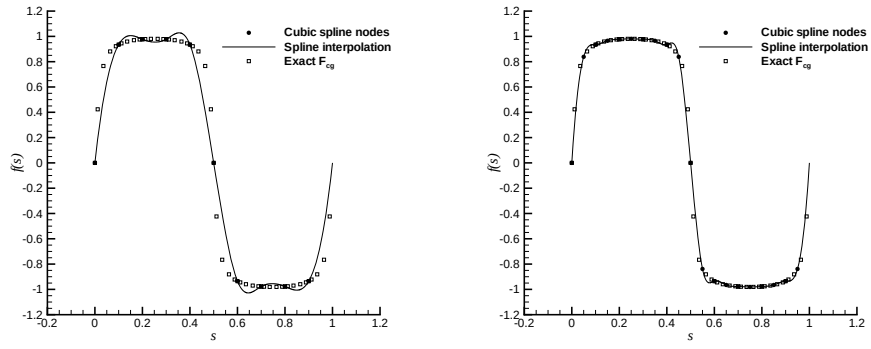

(a) $n_d - 1 = 10$ design points

(b) $n_d - 1 = 20$ design points

Fig. 5 Effect of the number of cubic spline design nodes ($n_d - 1$) on the accurate simulation of $f(s) = \arctan(10 \sin 2\pi s)/1.5$. The interpolation error of the force values at GLL points (F_{cg}) is reduced by increasing n_d.

The optimization problem is solved using a gradient-based optimization method provided by the *fmincon* function in Matlab [30], where the gradient of the objective

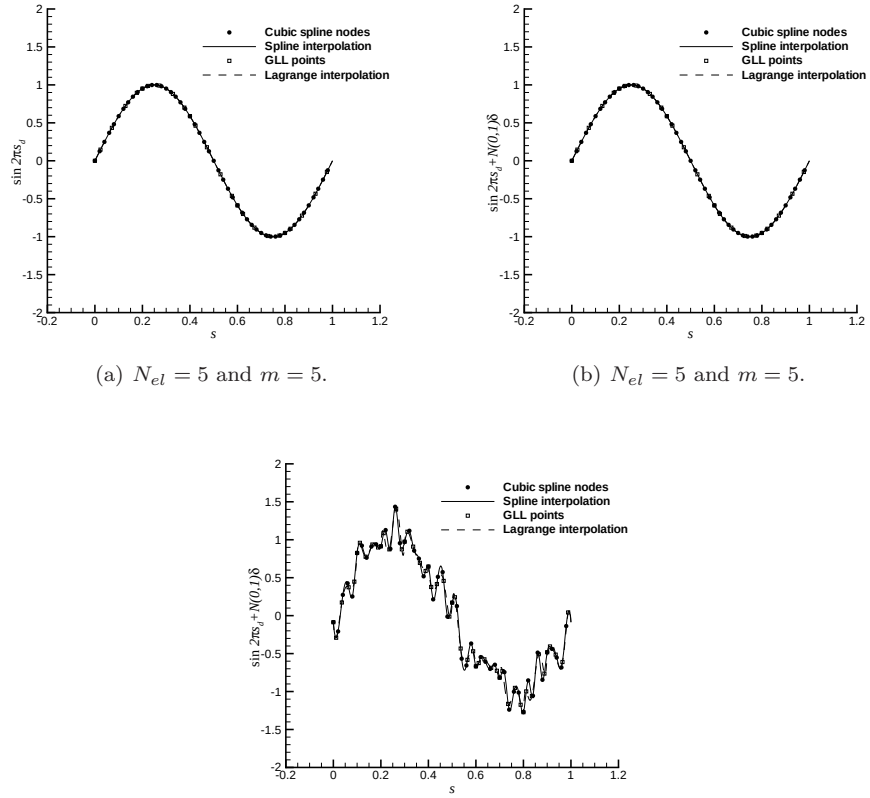

(a) $N_{el} = 5$ and $m = 5$.

(b) $N_{el} = 5$ and $m = 5$.

(c) $N_{el} = 10$ and $m = 5$.

Fig. 6 Inaccurate time integration due to under-resolution in the spectral element discretization for a design perturbation.

function is used to guide the optimization search. The gradient can be computed using direct, adjoint or finite-difference methods. The last method is more vulnerable to round-off error in the cost function and is computationally expensive. For example, the gradient is computed using central finite-difference with respect to each design variable, b according to

$$G_d = \frac{W(F_d + \delta b) - W(F_d - \delta b)}{2\delta b}, \tag{54}$$

where G_d is the gradient of W at design node d. Because W is not available analytically, its value can be estimated using numerical integration. The integral of (51) is computed using Gauss quadrature formula according to (9). A numerical error ϵ_w may result in the calculation of W. When the number of control force design variables increases, the round-off error start to dominate the computed value of W and ϵ_w becomes significant [2, page 257]. This causes the gradient to exhibit a numerical noise. Alternatively, the gradient can be computed using the direct method or adjoint

methods. Using direct method the gradient of W

$$\frac{\partial W}{\partial b} = \int_0^1 \left[\frac{\partial F_g}{\partial b} \cdot X_{cg} + F_g \cdot \frac{\partial X_{cg}}{\partial b} \right] ds. \tag{55}$$

The direct method is computationally more expensive than the adjoint method for a large number of design variables. To derive the adjoint equation, we write the equation of motion (20) in the form

$$X_{cg} = \boldsymbol{C} F_{cg}. \tag{56}$$

The adjoint sensitivity is then derived by adding the dot product of an adjoint vector λ with the gradient of (56) to (55)

$$\frac{\partial W}{\partial b} = \int_0^1 \left[\frac{\partial F_g}{\partial b} \cdot X_{cg} + F_g \cdot \frac{\partial X_{cg}}{\partial b} \right] ds + \int_0^1 \lambda \cdot \left[\frac{\partial X_{cg}}{\partial b} - \boldsymbol{C} \frac{\partial F_{cg}}{\partial b} - \frac{\partial \boldsymbol{C}}{\partial b} F_{cg} \right] ds, \tag{57}$$

where to eliminate the need to compute $\frac{\partial X_{cg}}{\partial b}$, the adjoint vector becomes

$$\lambda = -F_g. \tag{58}$$

The adjoint sensitivity is then

$$\frac{\partial W}{\partial b} = \int_0^1 \left[\frac{\partial F_g}{\partial b} \cdot X_{cg} \right] ds - \int_0^1 \lambda \cdot \left[\boldsymbol{C} \frac{\partial F_{cg}}{\partial b} + \frac{\partial \boldsymbol{C}}{\partial b} F_{cg} \right] ds. \tag{59}$$

Although the computation of $\frac{\partial \boldsymbol{C}}{\partial b}$ is expensive to evaluate, it is only evaluated once for the control force period design variable and is zero for the control force design variables, F_d. The sensitivity of the constraint (49b) is computed using the adjoint method according to (34), where the adjoint vector is computed according to (33) and $\boldsymbol{y}$ is the identity matrix. Once the sensitivity of the GLL response points to each design variable is evaluated, the sensitivity of the critical point constraint is calculated by inserting the critical time (evaluated separately using a one dimensional optimization search similar to the absorber problem) into a SE trial solution (4).

To mitigate the effect of the numerical noise in the computed gradient for the control force design nodes, a smoothing method can be used [36], where a smoothed gradient $\bar{G}$ is computed from the calculated gradient G according to

$$\bar{G} - \epsilon \frac{\partial^2 \bar{G}}{\partial s^2} = G. \tag{60}$$

The smoothing parameter ϵ is selected to average out the numerical noise without losing significant information in G. In implementing the finite-difference smoothing in Eq. 60, we note because of the periodic boundary condition, the gradient at $(s = 0)$ is equal to the gradient at $s = 1$. The gradients of the objective and constraint functions are computed in Figures 7, respectively. The constraint function correspond to the critical points (maximum and minimum) in the response. The control force is a cosine function with a period, $T = 1.3T_n$. Due to the large number of design nodes, $n_d = 121$ some numerical error is apparent in the computed gradients. To filter out the noise in the gradient, a smoothing is applied with $\epsilon = 0.005$ and is shown effective in removing the numerical noise. When the number of design nodes is not high, $n_d = 31$, the numerical noise in the gradients is nonexistent as demonstrated in Figures 8. The variation noted near the boundary is probably not due to round-off errors, though the smoothing is

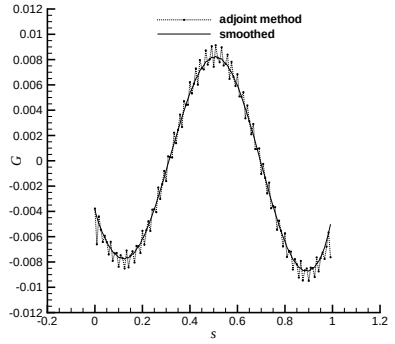

(a) Maximum critical point.

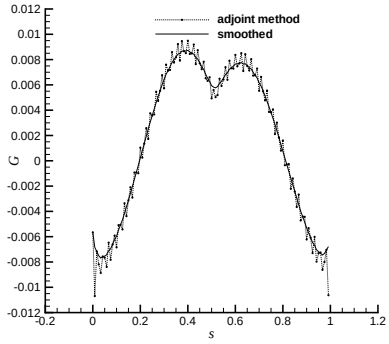

(b) Minimum critical point.

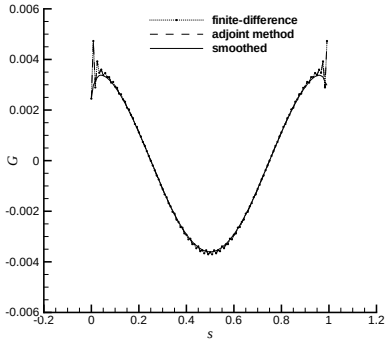

(c) Work objective.

Fig. 7 Gradients of the objective and constraints for the maximum and minimum critical points. The smoothed gradient is computed using $\epsilon = 0.005$ and is found effective in reducing numerical noise.

effective in filtering out this oscillation out. Note that the finite-difference and adjoint sensitivities of the objective function coincide for both $n_d = 31$ and $n_d = 121$.

The standard procedure of scaling the objective function, displacement constraints and range of design variables is implemented to enable an efficient optimization search, where convergence of the gradient-based method may be adversely affected when using different length scales of the design variables [37]. Here we normalize the objective function and displacement by the difference of their corresponding values at the natural period and $T_n/4$ of the system, for the initial control force. Parameters which remain fixed in all the following calculations are listed in Table 3 unless specified otherwise. Now, we report results of the optimization search for a different initial designs, where the gradients are computed using the adjoint method.

Initially we analyze the optimization search regarding the effect of using different initial designs of the control force for a constant initial period $T_i = 1.5T_n$. Table 4 reports on the optimization search with respect to the target displacement amplitude, Z_T, initial work W_i, optimum work, W_o, initial displacement amplitude, Z_i,

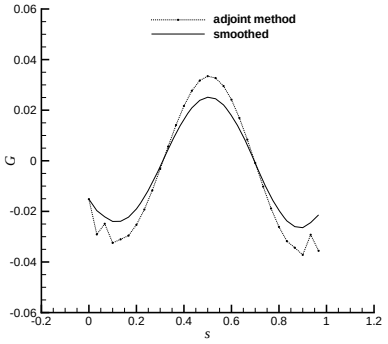

(a) Maximum critical point.

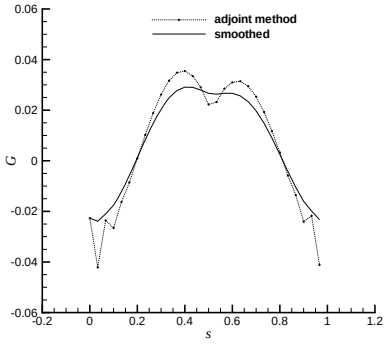

(b) Minimum critical point.

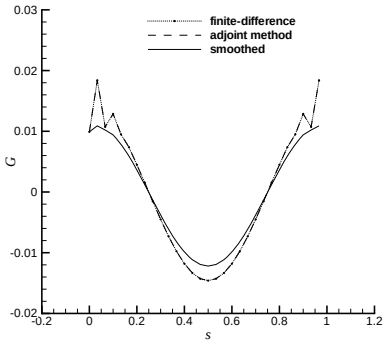

(c) Work objective.

Fig. 8 Gradients of the objective and constraints for the maximum and minimum critical points. Significant variation occur near the boundary, but is not due to round-off error. Gradient smoothing with $\epsilon = 0.005$ is effective in dampening this variation.

Table 3 Fixed parameters of the control force problem.

M (kg)	K (N/m)	C (N.s/m)	T_n (s)	n_d	m	N_{el}
0.010	10	0.012	0.199	31	5	30
Objective tolerance 1×10^{-6}		Constraint tolerance 1×10^{-6}		Design tolerance 1×10^{-6}		

optimum control force period, T_o and optimization cost (number of function evaluations and iterations of the *fmincon* function). Three functional forms of the initial control force are considered namely: $\sin 2\pi s$, $\cos 2\pi s$ and $\arctan(10 \sin 2\pi s)/1.5$. The final designs of the control force shapes are reported in Figure 9. It is observed that the $\arctan(10 \sin 2\pi s)/1.5$ initial design converges to the optimum solution in the least numbers of iterations and function evaluations. Although all solutions have an approximately equal optimal work objectives and forcing periods, the optimal control force

of the $\cos 2\pi s$ function differs in phase from the $\sin 2\pi s$ and $\arctan(10 \sin 2\pi s)/1.5$ functions.

The effect of the initial guess of the forcing period on the optimization search is considered in Table 5, for a control force initial design corresponding to $\cos 2\pi s$. The final designs of the control force are reported in Figure 10. In the first three cases, the target amplitude is held constant $Z_T = 1$, while the initial guess of the forcing period, T_i is varied. The results indicate that the optimal work and period of the control force is almost unchanged, but the control force exhibits different amounts of overshoot between the control force nodes. This overshoot is further analyzed in Figure 11 for case 2 in the table. The overshoot seem to diminish when a higher number of design variables are used $n_d = 61$. No gradient smoothing was needed here for convergence. Additionally, when the number of design variables is further increased $n_d = 121$, the overshoot is eliminated, though a gradient smoothing of $\epsilon = 0.005$ (for objective and constraints) was essential for convergence. In both cases the optimal work and period were $W_o = 1.109$ N.m and $T_o/T_n = 1.0673$, which are close to the one reported for case 2 in the table. For cases 4 and 5, the target amplitude is held at $Z_T = 0.5$, while using different initial guesses of the forcing period. It is observed that for $T_i/T_n = 1.5$ the optimal control force did not favor a regular design (square wave). Using a higher number of design variables $n_d = 61$, not reported here, converged to a saw tooth type of control force, but with $W_o = 0.297$ N.m and $T_o/T_n = 0.9839$. This indicate the existence of multiple solutions in the control force path and the sensitivity of the optimization search to initial guess of the control force period. Consequently, when the initial guess of the forcing period was closest to the optimal forcing period $T_i = T_n$, the optimization search had the least number of iterations to converge.

Finally we run the optimization search for a set of target displacement amplitudes. This allows us to compute the trade-off curve of the exerted work per cycle normalized by the optimal period (power) and maximum displacement amplitude Z_T. The calculation of the trade-off curve is computationally more expensive than a weighted sum approach, however, it allows the designer to select an optimum design based on his/her preferences, where a small increase in the amount of required power may yield larger increase in the target displacement.

An initial control force according to $\cos 2\pi s$ is used to compute the trade-off curve (Pareto front), see Figure 14. Different values of the control force period are used in the optimization searches. For $Z_T = \{0.5, 0.565\}$ a $T_i = 1.1T_n$ was used to enable convergence of the control force to a regular shape of the control force (similar to case 4 in Table 5). For the remaining amplitudes, the initial period is held constant at $T_i = 1.5T_n$, except for $Z_T = 3.3$, where an initial guess $T_i = 1.5T_n$ led the optimization search to an infeasible design, with the control force period being larger than its upper bound. However, when $T_i = 1.2T_n$ is used, convergence is possible to a regular control force (square wave). The optimum actuation period, see Table 6, is found larger than the natural period of the system, with the difference decreasing in magnitude (reported results are rounded to five significant figures) with increase in the maximum target amplitude. The final designs of the optimum control forces for each design on the Pareto front are shown in Figures 12 and 13. For the current system, there is an inherent dependence between the work per period and the displacement amplitude [38], consequently an initial control force design may already be close to the Pareto front. For example, the initial design for $Z_T = 0.5$ is close to the Pareto front. To realize the amount of improvement in this initial design, an optimization search is carried out where the target amplitude is equal to the initial amplitude, $Z_T = 0.565$ (second

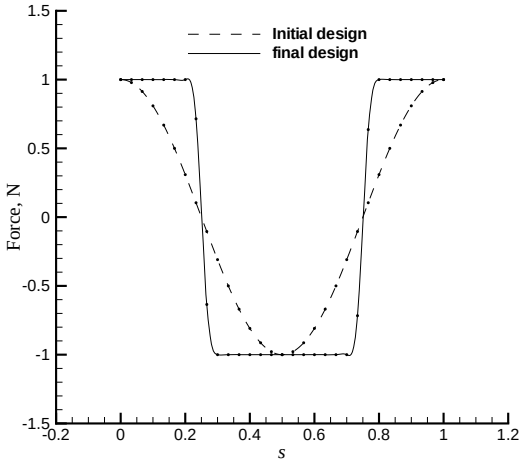

(a) $\cos 2\pi s$.

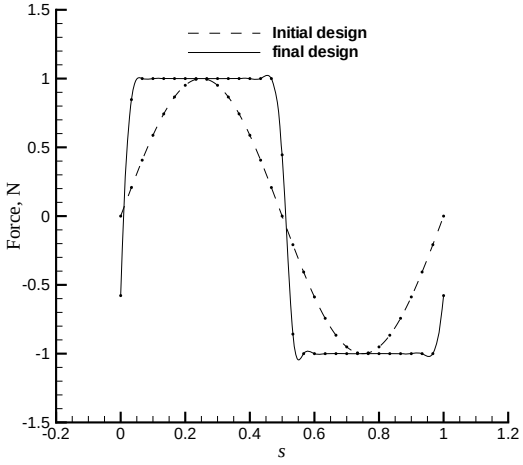

(b) $\sin 2\pi s$.

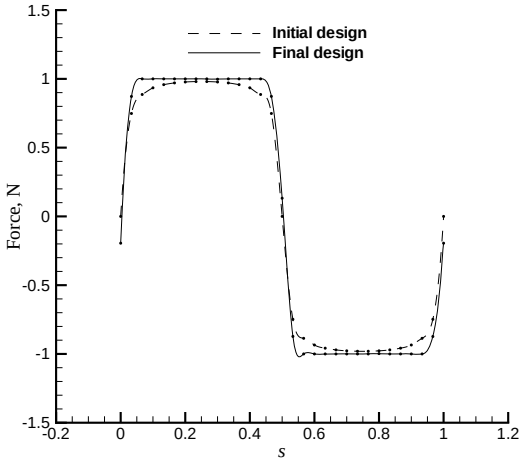

(c) $\arctan(10 \sin 2\pi s)/1.5$.

Fig. 9 Final designs of the control force for the initial designs given in Table 4.

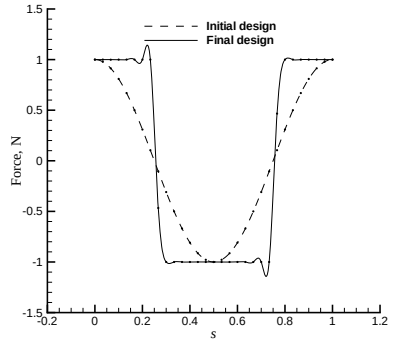

(a) $T_i/T_n = 0.5$, $Z_T = 1.0$.

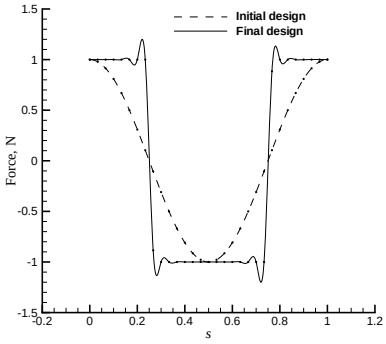

(b) $T_i/T_n = 0.8$, $Z_T = 1.0$.

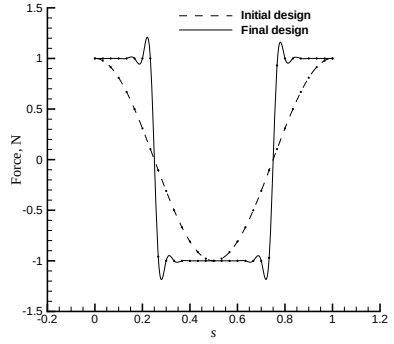

(c) $T_i/T_n = 1.0$, $Z_T = 1.0$.

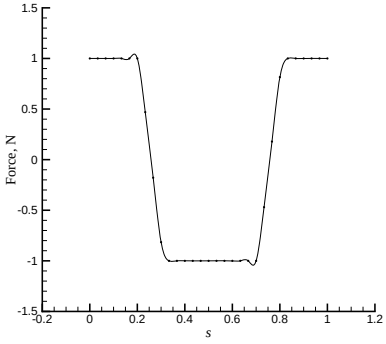

(d) $T_i/T_n = 1.1$, $Z_T = 0.5$.

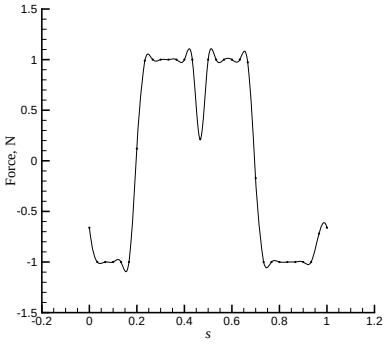

(e) $T_i/T_n = 1.5$, $Z_T = 0.5$.

Fig. 10 Final designs of the control force with a cosine function initial design, see Table 5.

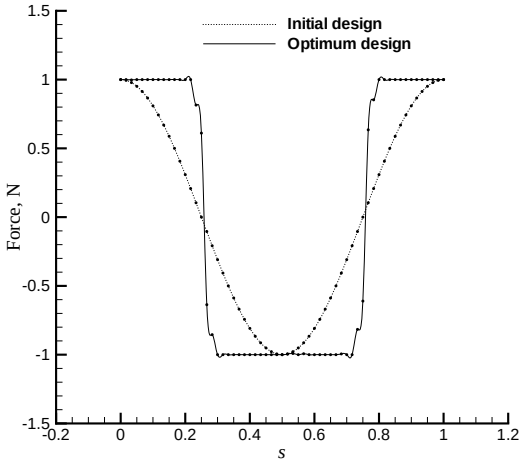

(a) $n_d = 61$ with no smoothing.

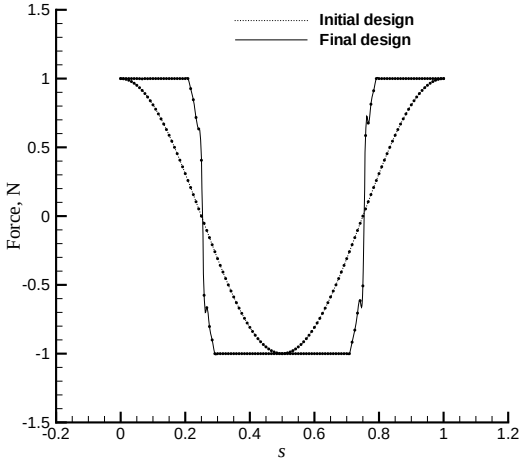

(b) $n_d = 121$ with smoothing, $\epsilon = 0.005$.

Fig. 11 Optimum control force for the initial design of case 2 in Table 5, but with higher design points, $W_o = 1.109$. The design variables constraint violation in between the design nodes is eliminated.

column in table). The total reduction in the power consumption from the initial design is around 7.5%. Here we alert the reader to the early version of the paper [39], where the minimum work is erroneously scaled by a 100.

Furthermore, the maximum target amplitude in the Pareto front $Z_T = 3.3$ m is not possible using a harmonic actuation force. The maximum amplitude for a harmonic

actuation of unit amplitude is [1, p. 52]

$$Z_{\max} = \left| \frac{1}{\sqrt{\left[1 - (T_n/T_{\max})^2\right]^2 + (2\zeta T_n/T_{\max})^2}} \right|, \tag{61}$$

where

$$T_{\max} = \frac{T_n}{\sqrt{1 - 2\zeta^2}}. \tag{62}$$

For the current system $T_{\max}/T_n = 1.0004$ and $Z_{\max} = 2.64$ m. This provides an approximately 25% improvement on the trivial initial design.

7 Conclusions

The optimization of systems for dynamic response is valuable in many applications. The performance function and/or constraints are governed by a time-dependent differential equation. In order to apply the time-dependent constraints or find the optimum cost function, the response is required for the whole time interval. In this paper, the response is computed in monolithic-time using a spectral element discretization, where the differential equation is transformed to an algebraic form. The search of the optimum design using gradient-based methods is simplified by the availability of the sensitivity of the time-dependent response to a change in the design variables explicitly. Depending on the problem, the sensitivity is computed using direct or adjoint methods.

Two optimization applications are described, the first one relates to transient analysis, where an impact absorber is designed to minimize the maximum acceleration. In this example we compare the accuracy and efficiency of applying the time-dependent constraints at GLL grid points to applying them at critical points (local extrema). The latter approach proved more efficient and accurate in computing the optimum solution.

The second application covers the periodic steady-state analysis. Here, the control force of a mass-spring-damper system is designed for minimum exerted work and maximum displacement amplitude. The system is a very simplified model of the control of micro air vehicles. The control force is simulated using a spline discretization with first derivative continuity, where the design variables are the control force period and the force magnitude at the spline nodes. Time-dependent response is computed for one period of the response using the spectral element method and the constraints are enforced at the critical points of the response. The study underlined the importance of effective selection in the number of design nodes in the spline and an adequate spectral element discretization. Increasing the number of design nodes in the spline, requires increasing the spectral element discretization to give accurate steady-state response for design perturbations. A high number of design nodes results in a round-off error in computing the cost function and contributes to numerical noise in the gradient.

Optimization results of the control force design favors a forcing period near the natural frequency of the system and a control force shape similar to that of a square wave. The sensitivity of the search to the initial guess in the control force period is observed, where an unfavorable initial period may yield to a non square form of the control force shape or an infeasible solution. The use of small number of design variables ($n_d = 31$) is found sufficient in approximating the control force variation over a cycle. However, some optimal designs exhibited an overshoot between the design

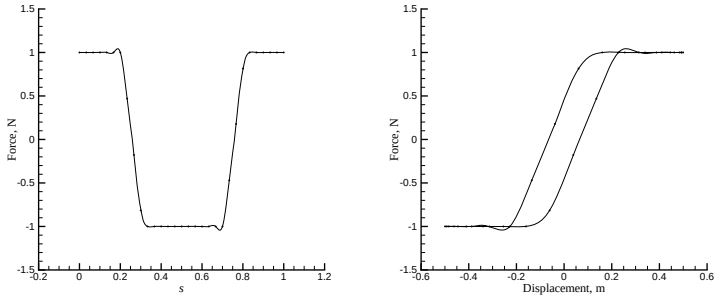

(a) $Z_T = 0.5$.

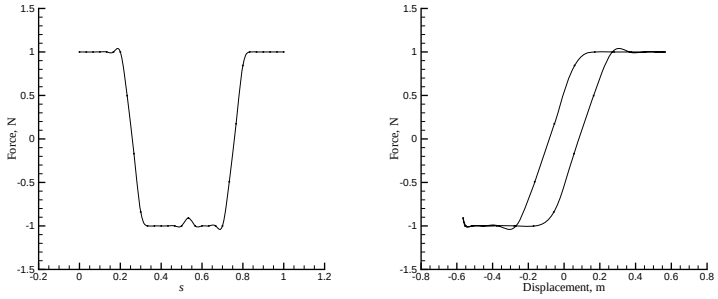

(b) $Z_T = 0.565$.

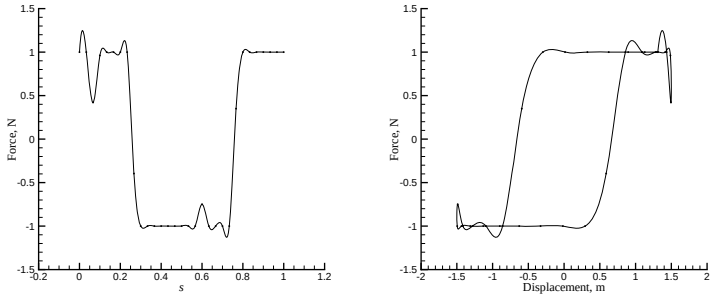

(c) $Z_T = 1.5$.

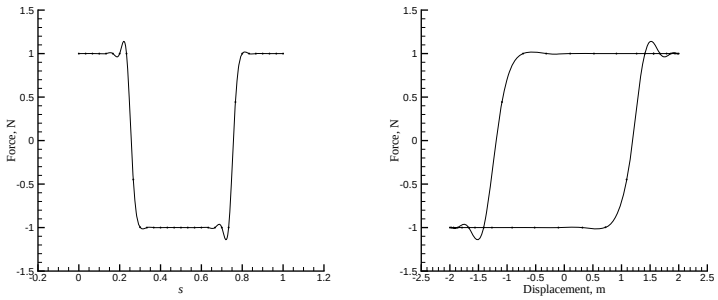

(d) $Z_T = 2.0$.

Fig. 12 Optimum control force for a specific target amplitude, Z_T.

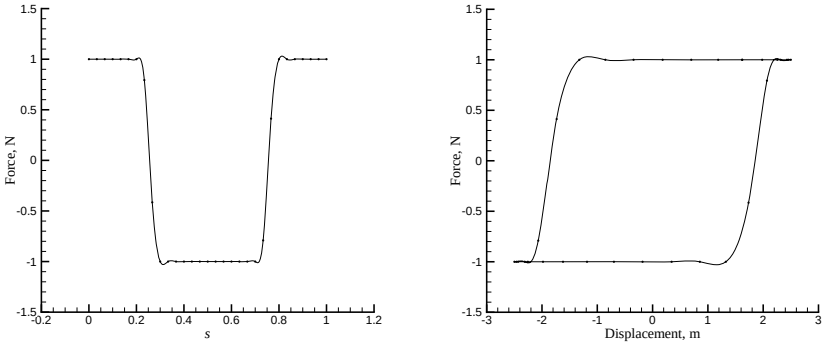

(a) $Z_T = 2.5$.

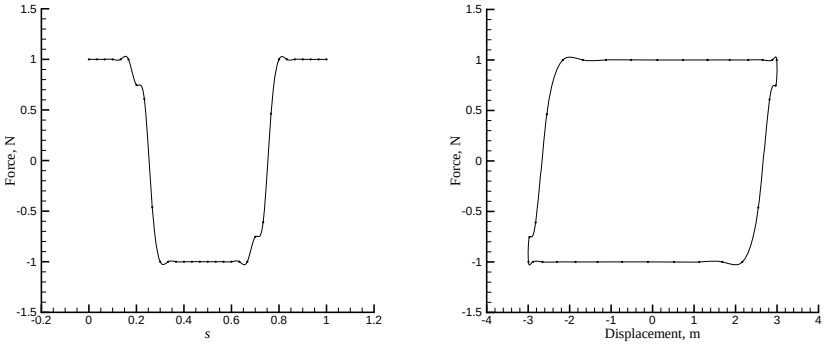

(b) $Z_T = 3.0$.

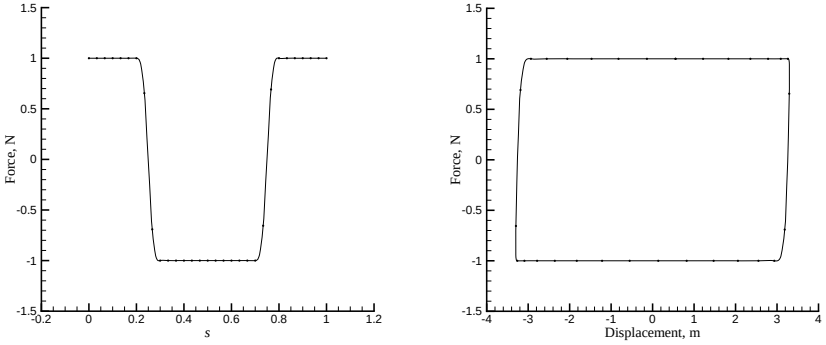

(c) $Z_T = 3.3$.

Fig. 13 Optimum control force for a specific target amplitude, Z_T.

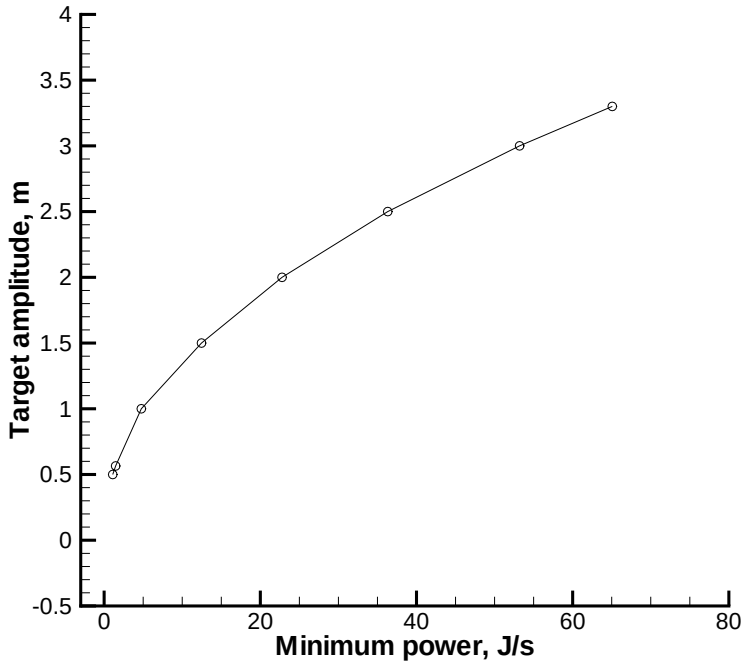

Fig. 14 Pareto front of applied work and target displacement amplitude.

nodes. Further analysis using higher number of design variables ($n_d = 61$ and $n_d = 121$) eliminated the overshoot, where a smoothed gradient was required for $n_d = 121$, due the noisy gradients.

Finally, the trade-off curve of the minimum work per cycle and maximum displacement amplitude is computed. The curve illustrate to the designer the amount of gain in the maximum displacement amplitude corresponding to an available minimum work per cycle. The optimum control force periods of the trade-off set is found to approach the natural period of the system with an increase in the target displacement amplitude. For initial designs close to the trade-off curve, the improvement in the work per cycle objective is found to be at around 7.5%.

The distinctive feature of the optimization approach used in the paper is the implementation of a high order spectral element computation of the dynamic response in a monolithic-time interval which includes the converged dynamics. The approach transforms the differential equation into an algebraic form, which enables a more explicit computation of the sensitivities as highlighted in the review by Kang et. al [4].

Acknowlegment This work is supported by the Air Force Office of Scientific Research under Grant 03VA01COR. We would like to thank our program manager Dr. Fariba Fahroo for her interest and financial support.

References

1. L. Meirovitch. *Elements of vibration analysis*. McGRAW-Hill, 1986.
2. R.T. Haftka and Z. Gurdal. *Elements of Structural Optimization*. Kluwer Academic Publishers, Dordrecht, The Netherlands, 1992.
3. C. C. Hsieh and J. S. Arora. Design sensitivity analysis and optimization of dynamic response. *Applied Mathematics and Optimization*, 43(2):195 – 219, 1984.
4. Byung-Soo Kang, Gyung-Jin Park, and J.S. Arora. A review of optimization of structures subjected to transient loads. *Structural and Multidisciplinary Optimization*, 31(2):81 – 95, 2006.
5. S. Park, R.K. Kapania, and S.J. Kim. Nonlinear transient response and second-order sensitivity using time finite element method. *AIAA Journal*, 37(5):613 – 622, 1999.
6. R.K. Kapania and S. Park. Nonlinear transient response and its sensitivity using finite elements in time. *American Society of Mechanical Engineers, Design Engineering Division*, 84(3 Pt B/2):931 – 942, 1995.
7. A.T. Patera. A spectral element method for fluid dynamics; laminar flow in a channel expansion. *Journal of Computational Physics*, 54:468–488, 1984.
8. M.H. Kurdi and P.S. Beran. Spectral element method in time for rapidly actuated systems. *Journal of Computational Physics*, 227(3):1809–1835, 2008.
9. J.H. Argyris and D.W. Scharpf. Finite elements in time and space. *Nuclear Engineering and Design*, 10(4):456 – 464, 1969.
10. I. Fried. Finite element analysis of time-dependent phenomena. *AIAA Journal*, 7:1170 – 1173, 1969.
11. J.P. Pontaza and J.N. Reddy. Space-time coupled spectral/hp least-squares finite element formulation for the incompressible Navier-Stokes equations. *Journal of Computational Physics*, 197(2):418 – 59, 2004.
12. C.M. Klaij, J.J.W. van der Vegt, and H. van der Ven. Space-time discontinuous Galerkin method for the compressible Navier-Stokes equations. *Journal of Computational Physics*, 217(2):589 – 611, 2006.
13. K.D. Wilmert and R.L. Fox. Optimum design of a linear multidegree-of-freedom shock isolation system. *Journal of Engineering for Industry*, 94:465 – 471, 1972.
14. K. A. Afimiwala and R. W. Mayne. Optimum design of an impact absorber. *Journal of Engineering for Industry, Transactions of the ASME*, 96 B(1):124 – 130, 1974.
15. V.B. Venkayya, N.S. Khot, V.A. Tischler, and Taylor R.F. Design of optimum structures for dynamic loads. In *the 3rd Conference on Matrix Methods of Structural Mechanics*, pages 619–658, Flight Dynamics Laboratory, Wright Patterson Air Force Base, Ohio, October 1971.
16. R.T. Haftka. Parametric constraints with application to optimization for flutter using a continuous flutter constraint. *AIAA Journal*, 13(4):471–475, 1975.
17. W.S. Choi and G.J. Park. Structual optimization using equivalent static loads at all time intervals. *Compuational Methods in Applied Mechanics and Engineering*, 191:2077–2094, 2002.
18. R.V. Grandhi, R.T. Haftka, and Layne T. Watson. Design oriented identification of critical times in transient response. AIAA Paper 1984-0899.
19. R.V. Grandhi, R.T. Haftka, and L.T. Watson. Efficient identification of critical stresses in structures subject to dynamic loads. *Computers and Structures*, 22(3):373 – 86, 1986.

20. N.H. Kim and K.K. Choi. Design sensitivity analysis and optimization of nonlinear transient dynamics. *Mechanics of Structures and Machines*, 29(3):351–371, 2001.
21. F. van Keulen, R.T. Haftka, and N.H. Kim. Review of options for structural design sensitivity analysis. part 1: Linear systems. *Computer Methods in Applied Mechanics and Engineering*, 194(30-33):3213–3243, 2005.
22. S.K. Nadarajah and A. Jameson. Optimum shape design for unsteady flows with time-accurate continuous and discrete adjoint methods. *AIAA Journal*, 45(7):1478–1491, 2007.
23. A. Jameson. Aerodynamic shape optimization techniques based on control theory. *Computational Mathematics Driven by Industrial Problems (Lecture Notes in Mathematics)*, 1739:151–221, 2000.
24. N.H. Kim. Eulerian shape design sensitivity analysis and optimization with a fixed grid. *Computer Methods in Applied Mechanics and Engineering*, 194(30-33):3291–3314, 2005.
25. G.E. Karniadakis and S.J. Sherwin. *Spectral/hp element methods for CFD*. Oxford University Press, 1999.
26. C. Pozrikidis. *Introduction to finite and spectral element methods using Matlab*. Chapman and Hall/CRC, 2005.
27. D.S. Burnett. *Finite element analysis; from concepts to applications*. Addison-Wesley, 1988.
28. L.F.P. Etman, D.H. Van Campen, and A.J.G. Schoofs. Design optimization of multibody systems by sequential approximation. *Multibody System Dynamics*, 2:393–415, 1998.
29. E.J. Haug and J.S. Arora. *Applied optimal design: mechanical and structural systems*. Wiley-Interscience, New York, 1979.
30. Mathworks, 2007a, Natick, MA.
31. W. Shyy, M. Berg, and D. Ljungqvist. Flapping and flexible wings for biological and micro air vehicles. *Progress in Aerospace Sciences*, 35(5):455 – 505, 1999.
32. P.S. Beran, R.D. Snyder, and M. Blair. A design optimization strategy for micro air vehicles. AIAA Paper 2007-1853.
33. K. Palaniappan, P.S Beran, and A. Jameson. Optimal control of LCOs in aero-structural systems. AIAA-2006-1621.
34. M. Kaya and I. H. Tuncer. Path optimization of flapping airfoils based on nurbs. *Parallel Computational Fluid Dynamics*, pages 285–292, 2007.
35. D.L. Raney and E.C Slominski. Mechanization and control concepts for biologically inspired mirco air vehicles. *Journal of Aircraft*, 41(6):1257–1265, 2004.
36. A. Jameson and J.C. Vassberg. Studies of alternative numerical optimization methods applied to the brachistochrone problem. *Computational Fluid Dynamics*, 9(3):281–296, October 2000.
37. J.F. Schutte, Byung-Il Koh, J.A. Reinbolt, R.T. Haftka, A.D. George, and B.J. Fregly. Evaluation of a particle swarm algorithm for biomechanical optimization. *Transactions of the ASME. Journal of Biomechanical Engineering*, 127(3):465 – 74, 2005.
38. R.F. Jr Steidel. *An introduction to mechanical vibrations*. John Wiley and Sons, 1989.
39. M.H. Kurdi and P.S Beran. Optimization of dynamic response using temporal spectral element method. AIAA-2008-0903.

Table 4 Effect of initial control force form on the optimization search for an initial period $T_i = 1.5T_n$ and target displacement amplitude $Z_T = 1$ m.

Case #	function	W_i	W_o	Z_i	T_i/T_n	T_o/T_n	# function evaluations	# iterations
1	$\cos 2\pi s$	0.026	1.009	0.180	1.5	1.0672	49	23
2	$\sin 2\pi s$	0.026	1.109	0.180	1.5	1.0673	55	26
3	$\arctan y/1.5$[§]	0.038	1.110	0.226	1.5	1.0669	17	7

[§] $y = 10 \sin 2\pi s$

Table 5 Effect of initial control force period on the optimization search with a cosine function initial design.

Case #	Z_T	W_i	W_o	Z_i	T_i/T_n	T_o/T_n	# function evaluations	# iterations
1	1	0.003	1.109	0.033	0.5	1.0675	87	42
2	1	0.047	1.108	0.177	0.8	1.0677	75	36
3	1	8.279	1.108	2.635	1.0	1.0678	36	16
4	0.5	0.346	0.253	0.565	1.1	1.1552	73	36
5	0.5	0.026	0.253	0.36	1.5	1.1445	227	89

Table 6 Pareto front optimal set.

Target amplitude, m	0.5	0.565	1.0	1.5	2.0	2.5	3.0	3.3
Minimum work, N.m	0.25	0.33	1.01	2.57	4.65	7.34	10.67	12.97
T_o/T_n	1.1552	1.1323	1.0672	1.0387	1.0268	1.0175	1.0091	1.0031
Minimum power, J/s	1.10	1.47	4.76	12.47	22.78	36.32	53.20	65.07
Initial amplitude, m	0.565	0.565	0.18	0.18	0.18	0.18	0.18	0.326
Initial work, N.m	0.35	0.35	0.03	0.03	0.03	0.03	0.03	0.11
Initial power, J/s	1.58	1.58	0.09	0.09	0.09	0.09	0.09	0.44
T_i/T_n	1.1000	1.1000	1.5000	1.5000	1.5000	1.5000	1.5000	1.2000